

Modified Photochemical Properties of Mitoxantrone by Plasmonic Photothermal Response of Hollow Gold Nanoshells

Armin Imanparast^{1,2}, Mohamadreza Diba³, Ameneh Sazgarnia^{*1,2}

1. Medical Physics Research Center, Mashhad University of Medical Sciences, Mashhad, Iran.

2. Department of Medical Physics, Faculty of Medicine, Mashhad University of Medical Sciences, Mashhad, Iran.

3. Master student of medical biochemistry, Shiraz University of Medical Sciences, Shiraz, Iran.

ARTICLE INFO

Article type:
Original Article

Article history:
Received: Jun 18, 2018
Accepted: Jul 16, 2018

Keywords:
Mitoxantrone
Nanoshells
Photodynamic
Photothermal

ABSTRACT

Introduction: Mitoxantrone (MX) has been introduced as a photosensitizer drug. However, due to some side effects, the widespread use of this drug has been confronted with some limitations. Hollow gold nanoshells (HGN) have attracted considerable attention due to their interesting photochemical features that can use as nanocarrier. In this paper, the thermal response of MX and the use of this property for thermal effects during the photodynamic process by MX-conjugated HGN were investigated.

Material and Methods: After optimizing the synthesis of ultimate nanostructure, the characteristics of pharmacological agents including MX, HGN, methoxy polyethylene glycol (mPEG)-HGN, and MX-mPEG-HGN were determined. Then, the thermal response of MX was determined at 0-50°C. Finally, by applying light irradiation with a non-coherent source at a wavelength of 670 nm and exposures of 0 to 50 J/cm², the profile release and temperature variation in MX-mPEG-HGN were determined.

Results: The zeta potentials of HGN and MX were negative, which resulted in electrostatic repulsion between them. In order to solve this challenge, the surface modification of HGN with mPEG was performed, resulting in the chemical bonding of the drug with the nanostructures and increasing the stability of the final nanostructure. With increasing temperature, the optical density of the drug at 660 nm significantly increased, which is an effective induction of photodynamic effect.

Conclusion: In this study, we used mPEG-HGN as the nanocarrier for MX. Also, the thermal behavior of MX was recognized as an important factor in increasing temperature that could improve the photodynamic process.

► Please cite this article as:

Imanparast A, Diba M, Sazgarnia A. Modified Photochemical Properties of Mitoxantrone by Plasmonic Photothermal Response of Hollow Gold Nanoshells. Iran J Med Phys 2019; 16: 56-63. 10.22038/ijmp.2018.32804.1397.

Introduction

Photodynamic therapy (PDT) is one of the non-invasive methods for selectively removing tumor cells. Starting the PDT process requires three essential factors including photosensitizer (PS), light source (with emission wavelength proportional to PS), and oxygen in the tumor site. These components are not toxic individually, but in simultaneous use for photodynamic processes, they lead to photochemical effects and toxicity. Photodynamic process products include reactive oxygen species (ROS) and singlet oxygen (¹O₂), which can cause cell death [1-3].

In recent years, chemo-photodynamic combination therapy has received widespread attention in cancer treatment due to its unique characteristics, such as its synergistic effects to improve therapeutic efficacy and reduce the adverse side effects of drugs [4]. As a chemotherapeutic agent, mitoxantrone (MX) has been used for the treatment of various malignancies, including acute myeloid leukemia [5], metastatic breast cancer [6], and non-Hodgkin's lymphoma [7]. MX is also used as a key factor in PDT and radiotherapy [8].

Most studies on the mechanism of MX demonstrated that nuclear and mitochondrial DNA are the main target for this drug [9]. MX has a planar anthraquinone ring in its structure and can intercalate between DNA base pairs. Also, this drug has a nitrogen-containing side chain that binds to the negatively charged phosphate groups of DNA. This assumption was supported by Foye et al. [10]. In the cell nucleus, DNA interacts with histones and builds complex structures named nucleosomes. Nucleosomes consist of 145 to 155-base pairs DNA wrapped around an octamer of histones (H1: Linker histone and H2A, H2B, H3, and H4: Core histones).

Histones are necessary to maintain the integrity of the genome, and any disruption in their activity leads to instability and creation of genetic lesions that increase tumorigenicity [11]. Double-stranded DNA in cancer cells are associated with histone proteins making nucleosomes, but because of epigenetic changes of chromatin, the structure is more relaxed compared to normal cells [12]. On the other hand, MX by attaching to histones and changing their structures causes the condensation of the DNA structure and

prevents replication, transcription, and thus, the division of cancer cells.

The important point is that MX has a higher tendency to histones than free double or single-stranded DNA [13]. MX also inhibits topoisomerase II that is the main enzyme repairing DNA damage. MX can also readily penetrate into cellular membranes by passive diffusion [14], which leads to the accumulation of the drug in cancer cells. MX has also been reported to interact with other cellular structures (e.g., cell cytoskeleton, specifically cytokeatin and lamin intermediate filaments). In vitro, MX binds with high affinity to tubulin and can subsequently inhibit its assembly into microtubules, which plays a major role in cellular division [15].

The inhibition of microtubule and cytoskeleton assembly by MX is a potential factor in its mechanism of action in cancer treatment [16]. Many studies have clearly demonstrated that MX inhibits macromolecular biosynthesis in cells [17]. In cultured mammalian cells, this drug strongly inhibited the incorporation of [3H]-thymidine and [3H]-uridine into DNA and RNA, respectively [18]. Thus, MX is a potent inhibitor of cellular and mitochondrial nucleic acid synthesis (Fig. 1) [19].

The entrapment of anticancer drugs into biocompatible nanostructures can control drug release, which increases their half-life in blood circulation. An ideal nanocarrier should have stable physicochemical properties including chemical stability, low toxicity, long half-life, biodegradation capabilities, and high conjugation capacity [20]. Gold nanostructures can be synthesized in a range of shapes and sizes such as core-shells, rods, cubes, wires, and triangles. They are generally synthesized

chemically using sodium borohydride, trisodium citrate dehydrate, and hydroquinone reduction of a chloroauric acid (HAuCl₄) solution. The type of reducing agents, the ratio of gold salt to reducing agent, and primary temperature play a critical role in determining the shape and size of gold nanostructures [21, 22].

Among many nanoscale materials, hollow gold nanoshells (HGN) offer excellent candidates for combination therapy due to their high efficiency of drug loading, good biological safety, biocompatibility, and functional ability [23]. The surface plasmon resonance band of HGN can be tuned in visible to near-infrared range by adjusting the hollow core/shell ratio.

Due to the unique physicochemical properties of HGN, they have multifunctional nanoparticles in medical applications. As contrast agents, biological compounds of HGN are used to identify and image tumor cells and solid tumors in vivo. HGN are also designed as photothermal agents to induce thermal necrosis of tumors in animal studies [24].

PEGylation process helps the foreign agent (e.g., nanocarrier) escape from the immune system by reduced risk of nanocarrier uptake by the reticuloendothelial system. The methoxy polyethylene glycol (mPEG)-thiol group can reduce the risk of formation of large agglomerates of nanostructures, increase the solubility of nanoparticles in aqueous media, enhance conjugation efficiency, lower nonspecific protein binding, and provide nanostructured surfaces as an amphiphilic environment for insoluble drugs in water (stealth effect) [25, 26].

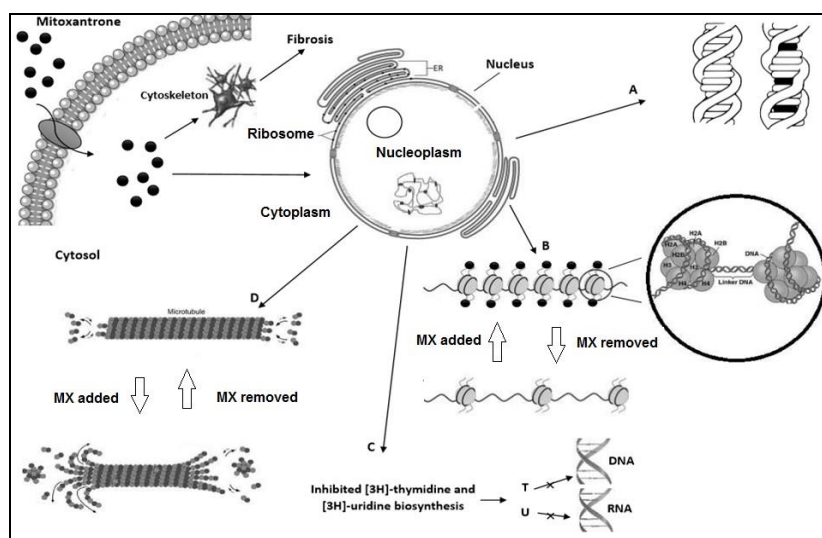


Figure 1. Mitoxantrone mechanism of action: Mitoxantrone (MX), can readily penetrate into cellular membranes by passive diffusion and interact with hydrophobic structures (for example cytoskeleton) and nucleus in cancer cells. In nucleus: A. MX can intercalate between DNA base pairs in DNA structure. B. MX by attaching to histones and changing their structures, causes the condensation of the DNA structure and prevents replication, transcription, and thus, the division of cancer cells. C. This drug also strongly inhibits the incorporation of [3H]-thymidine and [3H]-uridine into DNA and RNA biosynthesis, respectively, and D. MX binds with high affinity to tubulin and can subsequently inhibit its assembly into microtubules.

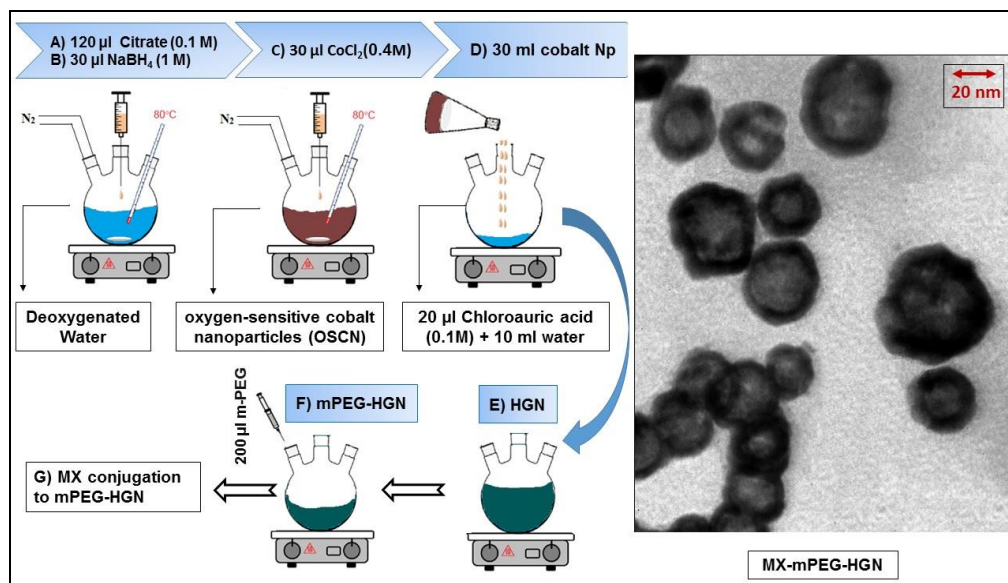


Figure 2. Synthesis scheme of hollow gold nanoparticles and the final product

Notes: (A, B) 120 µl of 0.1 M sodium citrate solution and 30 µl of 1 M sodium tetrahydroborate solution were added to 30 ml of deoxygenated ultra-pure water simultaneously. (C) Addition of 30 µl of a 0.4 M cobalt chloride solution (Synthesis of cobalt nanoparticle). (D) Cobalt nanoparticle was immediately transferred to a vortexing solution of 10 ml of deoxygenated ultra-pure water containing 25 µl of 0.1 M chloroauric acid. (E) Formation of hollow gold nanoshells. (F) 200 µl aqueous solution of methoxy-PEG was added to 19.8 ml of the HGNs solution. And (G) mitoxantrone conjugation to mPEG-HGN (diameter \approx 30-40 nm).

In this study, HGN was used to encapsulate MX, and after mPEGylation the nanostructure, its thermal and optical properties at different concentrations were evaluated using different exposures of an incoherent light source at 670 nm to release the drug from nanostructures into an aqueous medium. We also discussed the effect of heat on the optical properties of MX and nanostructures.

Materials and Methods

Chemicals

Cobalt chloride hexahydrate (99.99%), MX hydrochloride (MW=517.4), chloroauric acid ($\text{HAuCl}_4 \cdot 4\text{H}_2\text{O}$), trisodium citrate dehydrate (>99%), methoxy-polyethylene-glycol (mPEG-SH, MW=2000), and sodium borohydride (99%) were purchased from Sigma-Aldrich (St. Louis, MO, USA).

Instrumentations

The main equipment used in this study were Milwaukee UV-Vis spectrophotometer (UNICO UV-2100, USA), pH Thermometer (MT609, Italy), sodium tetrahydroborate (NaBH_4 ; 37.83 g/mol), radiometer (CON-TROL-CURE IL1400, USA), dynamic-light-scattering (DLS) particle size analyzer (Nano-ZS, Malvern, UK), incoherent light source (Lumacare, Newport Beach CA, USA; two probes with the wavelengths of 670 ± 25 and 730 ± 25 nm), light emitting diode (633 ± 13 nm; 3W), Philips CM120, and transmission electron microscope (TEM).

Synthesis of HGN and PEGylation

First of all, it should be noted that the water used in all stages of the hollow gold nanoshell synthesis should have three important features, that is, sterility, ultra-purity, and de-oxygenation, at all stages. The use of argon (or nitrogen) gas flux during the synthesis process is required to remove oxygen from the solution and prevent oxygen entry. For synthesizing HGN, we first synthesized cobalt nanoparticles as the sacrificial core. For this purpose, 120 µl of 0.1 M sodium citrate solution and 30 µl of 1 M NaBH_4 solution were added to 30 ml of deoxygenated ultra-pure water simultaneously. After a few seconds, with the addition of 30 µl of a 0.4 M CoCl_2 solution, a brown solution appeared due to the synthesis of cobalt nanoparticles. To increase the reaction speed and reduce the size of the primary cobalt nanoparticles, the synthesis process of cobalt nanoparticles was carried out at 80°C. In the next step, cobalt nanoparticles were immediately transferred to a vortexing solution of 10 ml of deoxygenated ultra-pure water containing 25 µl of 0.1 M gold salt (chloroauric acid). In this reaction, gold shells were formed on the surface of cobalt nanoparticles.

Finally, the solution was exposed to air or oxygen flux for oxidation and removal of the cobalt nanoparticle as a sacrificial core. The color of solution changed from brown to dark green indicating the oxidation of cobalt nanoparticles, which eventually led to formation of HGN (NS) [14].

To PEGylate the hollow gold nanoshells (P-NS), a 200 µl aqueous solution of mPEG was added to 19.8 ml of the HGNs solution on a magnet stirrer at room temperature for 4 h. The solutions were then centrifuged at 700 g for 15 min. The supernatant was gradually discarded to remove

excess mPEG, and then up to 5 ml of phosphate-buffered saline (PBS) solution was added (Figure 2).

Characterization of MX and nanostructures

The absorption spectra of MX, NS, P-NS, and MX-P-NS were recorded by an UV-Vis spectrophotometer. The particle size distribution, zeta potential, polydispersity index (PDI), and conductivity of the nanostructures were determined using a DLS. TEM imaging was used to examine the morphology of nanostructures.

Entrapment and release process of MX

The entrapment methods of the drug in hollow gold nanoshells include drug loading into the cavity space of nanoshells and drug conjugation (adhere) to the surface of nanoparticles. Spectrofluorimetric analyses were used to evaluate the entrapment and release process of MX from the mPEG-HGN. To study the entrapment process, fluorescence spectra of MX@mPEG-HGN (MX-P-NS) were recorded before and after the drug entrapment process. Along with the analysis of drug release, MX-P-NS (3×10^{11} particles/mL) was placed in a 24-well plate (the diameter of the source was equal to the diameter of the plate wells) and irradiated with a Lumacare (670 nm) at different exposure doses and subjected to spectrofluorimetric analysis immediately after irradiation with a Shimadzu spectrofluorimetric (Nakagyo-ku, Japan) at an excitation wavelength of 607 nm and emission spectrum of 665–705 nm. The following formula was used to calculate the exposure (power density= 65 mW/cm²):

$$\text{Exposure (J/cm}^2\text{)} = \text{power density (W/cm}^2\text{)} \times \text{time of irradiation (s)} \quad (1)$$

Judgment indexes

Photodynamic induction factor (PIF) was determined as a fraction of the optical density of MX at a desired temperature (OD [T°C]) to the optical density at room temperature (OD[25°C]) in a specific light wavelength and specific concentration of the agent. This factor

indicates that if the temperature rises, how does the optical density change and affect the efficacy of PDT.

$$\text{PIFMX(C)} = \frac{\text{OD(T}^\circ\text{C)}}{\text{OD(25}^\circ\text{C)}} \quad (2)$$

Results

Characterization of MX@mPEG-HGN

The results of TEM indicated that the synthesized nanostructures were hollow and had a mean diameter of 40 nm (Fig. 2). Physical characteristics of agents including size, zeta potential, conductivity, and polydispersity index (PDI) are shown in Table 1. MX zeta potential in aqueous solution (pH = 7) was about -15, but the zeta potential of HGN in the same conditions was -21 (Fig. 3, Table 1).

Since the zeta potentials were symptomatic (both were negative), the presence of electrostatic bond was excluded. Surface modification by mPEG led to a reduction of conductivity from 0.173 mS/cm to 0.069 mS/cm, zeta potential increased to near zero, and average size increased from 52 ± 4 to 74 ± 7 nm.

Considering the above factors, we concluded that the PEGylation process changed the physical properties of the primary HGN. PEGylation of HGN improved their colloidal stability in aqueous medium, resulting in no accumulation at room temperature for four months. Also, due to the reach out of the mPEG-HGN zeta potential to zero, the electrostatic repulsion effect between the mPEG-HGN and MX can be ignored, and the chemical bond between mPEG-HGN and MX is predictable, which causes the trapping of the MX and increases the efficiency of conjugation. Conjugation process increased the size of the nanoparticles up to 85 nm, changed conductivity to 0.273 mS/cm, and reached zeta potential to -12.4 mV. PEGylation and conjugation processes reduced the PDI index that shows the final product in an aqueous medium has good dispersity. Fig. 3 shows the variation in the zeta potential of the MX at various pH values.

Table 1. Physical characteristics of nanostructures (pH= 7)

Nanostructure	Size (nm)	Polydispersity index	Conductivity (mS/cm)	Zeta potential (mV)
HGN	52 ± 4	0.375 ± 0.031	0.173 ± 0.008	-21.6 ± 2.1
P-HGN	74 ± 7	0.271 ± 0.011	0.069 ± 0.004	-0.2 ± 0.8
MX-P-HGN	85 ± 4	0.174 ± 0.057	0.273 ± 0.009	-12.4 ± 1.7

Data are shown as mean \pm SD (n=4).

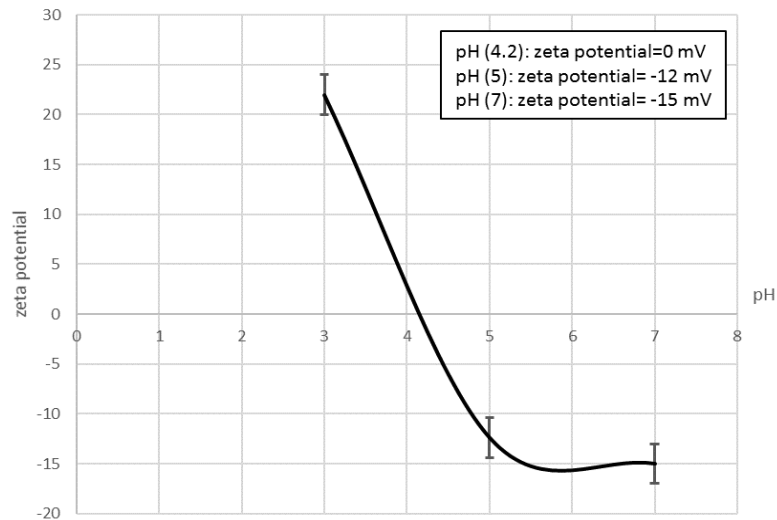


Figure 3. Zeta potential of mitoxantrone at different pHs. At pH values less than 4.2, the mitoxantrone zeta potential has positive values and zeta potential has a negative value at pH values greater than 4.2. Data are shown as mean \pm SD (n=4).

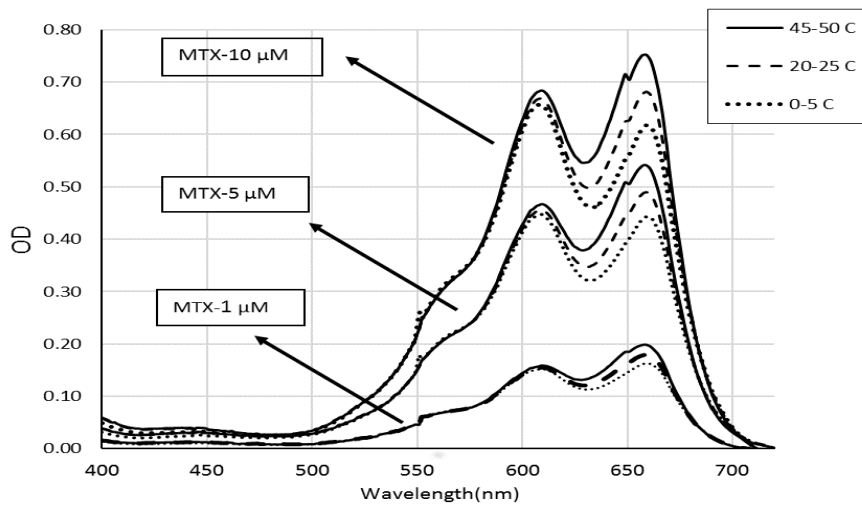


Figure 4. Optical density (OD) variations of mitoxantrone with increasing temperature from 0 to 50 °C. (n =4; repeat of the experiment)

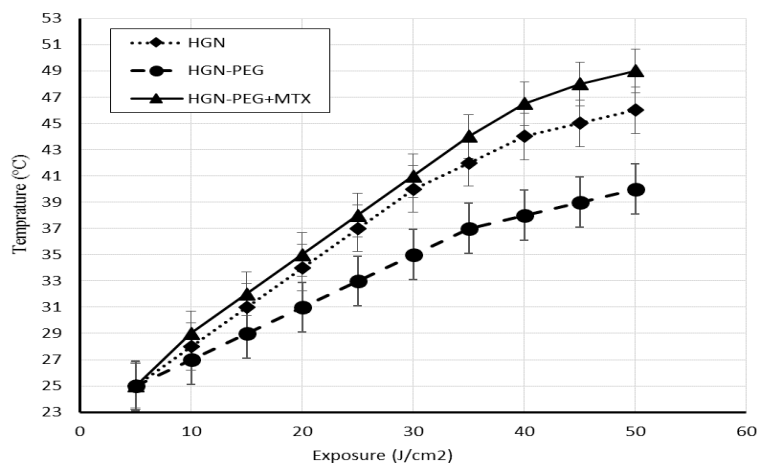


Figure 5. Temperature variations of different nanostructures with increasing irradiation dose. (n =4; repeat of the experiment)

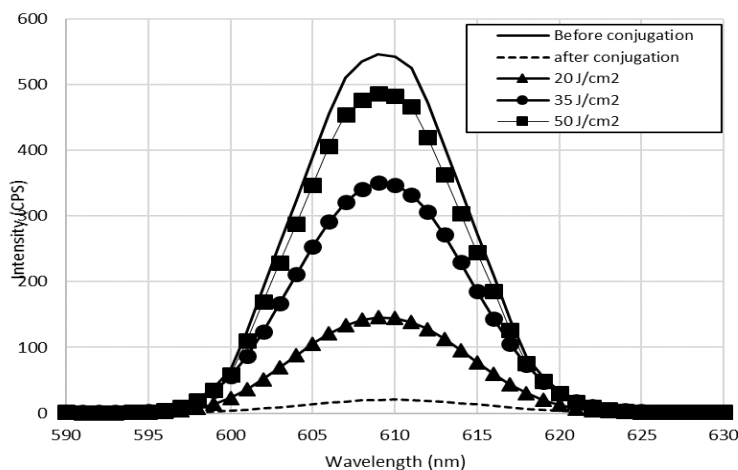


Figure 6. Fluorescence signal emission (FSE) variations during the mitoxantrone conjugation process and irradiation of different light exposures. An increase in the fluorescence signal level after radiation can be due to the release of the drug. ($n=4$; repeat of the experiment)

Thermal Behavior of the MX and MX-mPEG-HGN

Free MX had two maximum absorbances at 610 and 660 nm. Optical density (OD) changes of absorption peaks of the MX depend on concentration and temperature. As shown in Fig. 4, at high concentrations ($>5 \mu\text{M}$), OD changes of MX in terms of temperature are more significant at the second absorption peak (660 nm) than the first absorption peak (610 nm). On the other hand, as shown in Fig. 5, the temperature of the solution containing nanostructures increases with increasing optical dose in the photodynamic process. Therefore, along with photodynamic therapy, thermal effect is also predictable during irradiation. By applying irradiation to an exposure of 50 J/cm^2 , the temperature of the MX-P-HGN is increased to 49°C . In fact, HGN also plays a role in the heating of MX. Considering Fig. 4 and 5, increasing the temperature of MX up to 50°C leads to an increase in OD of MX, which can create a photodynamic induction effect. To quantify this claim, photodynamic induction factor was defined. The PIF at 670 nm (wavelength of the radiation source used in this study) was approximately 1.1 (Table 2).

Table 2. Photodynamic induction factor for different drug concentrations

Photodynamic induction factor (PIF)	670 nm
$\text{PIF}_{\text{MTX}}(1 \mu\text{M})$	1.05
$\text{PIF}_{\text{MTX}}(5 \mu\text{M})$	1.09
$\text{PIF}_{\text{MTX}}(10 \mu\text{M})$	1.11

MX release from MX@mPEG-HGN

Free MX exhibited strong fluorescence signal emission (FSE). Before the entrapment process of MX, the FSE of MX-P-NS was lower than that of free MX. After 24 hours, the FSE of MX-P-NS was almost completely quenched. The quenching phenomenon usually occurs when fluorophores parts of the drug are conjugated to or enclosed within the nanostructure. This

finding suggests the strong binding of MX to mPEG-HGN (Fig. 6).

FTIR spectra of MX@mPEG-HGN

In general, FTIR spectra can be divided into four regions in order to better interpret the infrared Fourier spectroscopy. The presence of distinct peaks in these regions indicates the functional groups absorbed in that range. The first region is from $4,000$ to $2,500 \text{ cm}^{-1}$ that the presence of characteristic peaks in the first region can be due to absorption through N-H, C-H, and O-H single bonds. The second region is between 2500 and 2000 cm^{-1} . If the spectrum has a characteristic peak in the range of second region, these peaks correspond to the absorption caused by triple bonds. The presence of characteristic peaks in the third region in the range from 2000 to 1500 cm^{-1} can be due to absorption by C=C, C=O, and C=N double bonds. One of the most important parts of the FTIR spectra is the fourth region (known as the fingerprint region) of the spectrum that is defined from the interval of 1500 to 400 cm^{-1} , which are associated with a large number of small and large peaks resulting from other single bonds.

According to FT-IR spectra of P-HGN and MTX-P-HGN in Fig. 7, the band seen at 1100 cm^{-1} was assigned to the C-N stretching vibration of MTX molecules on the surface of nanostructures. Also, the band existing at 1400 cm^{-1} was assigned to the C=C ring stretching vibration. The existence of a peak in the region of 1589 cm^{-1} was due to the C=C-C bond (aromatic ring bonding). The presence of one peak at 3425 cm^{-1} in the FT-IR spectrum of the nanoconjugation corresponds to N-H stretching vibration of MTX molecules. Therefore, the above data suggest that MTX conjugated on P-HGN [27].

Discussion

So far, no studies have been carried out on the use of hollow gold nanoshells conjugated with MX in PDT or

photothermal therapy (PTT), but the current study can be examined from two different perspectives, that is, investigating the use of MX as a photosensitizer in photodynamic or photothermal treatments and investigating the properties of MX conjugated to nanostructures and their specific goals in order to reduce toxicity and enhance cellular retrieval.

Montazerabadi et al. found for the first time that MX could be an important photosensitizer for PDT, such that this drug can produce significant cell death in concentrations of less than 5 μM and at a moderate optical dose in MCF-7 [8].

Boon et al. synthesized nanodiamonds (NDs; carbon polyhedron nanostructures) as a carrier of MX. NDs-MX by inhibiting efflux drug pumps leads to increased cellular uptake of MX in MDA-MB-231 cells. The amount of drug release from the NDs-MX is heavily dependent on pH variation and concentration of soluble proteins in the medium. The main goal of that study was enhancing therapeutic efficiency by inhibiting the expression of ABCG2 efflux receptors pumping the drug out of cancer cells [28].

Barrar et al. designed MX-loaded PEGylated magnetic nanoparticles used for theranostic (a combination of diagnostics and therapy) application in various cancers. They synthesized PEG-MNPs conjugated with folic acid (FA) as a linker and MX by covalent bonds to FA. The PEG-FA-MX-MNPs destroyed cancer cells by targeting folate receptors, increased the expression of BCL-2 and Caspase9, and reduced the expression of Akt [29].

In this study, the absorption peaks of HGN and MX at a wavelength of 660 nm were consistent. With optical irradiation at a wavelength of 670 nm with a relatively large bandwidth, the following phenomena can occur simultaneously:

- 1) The occurrence of photodynamic process by MX and the plasmonic photothermal phenomenon of nanoparticles simultaneously. Plasmonic photothermal therapy (PPTT) or plasmonic photothermal phenomenon occurs when there is a large overlap between the wavelength of the optical source and the nanostructure absorption peak. In this case, light irradiation leads to surface electron resonance of nanostructures and increases temperature [30].
- 2) The excessive increase in the temperature of the MX-mPEG-HGN causes release of the drug and the increase of the soluble temperature, which in turn, activates MX thermal response and increases optical density at the absorption peak of 660 nm. This phenomenon results in a further elevation in the temperature of the solution containing nanoparticles and drugs.

Conclusion

Hollow gold nanoshells according to their attractive features, provide unique capabilities for combination treatments including PDT, photothermal therapy, and chemotherapy. The most important advantage of gold

nanoparticles in photodynamic-photothermal treatments can be the ability to adjust the surface plasmon resonance band from visible to infrared.

In this study, for the first time, the thermal behavior of MX was discussed. It is proven that under certain conditions, it can act as an exacerbating factor in the photodynamic process. As the temperature increases, MX optical density at 660 nm increases. This represents a unique behavior depending on the temperature. Increasing optical density without increasing concentration is a key behavior that can enhance the benefits of photodynamic and photothermal effects. On the other hand, in this study, mPEG-HGNs were used as carriers of the drug and the main intermediates for increasing MX temperature.

The most important results of this study was that the optical density of MX at 660 nm was more sensitive to temperature than other wavelengths, which if used with a 660-nm emission light source, would increase the photodynamic efficiency along with the occurrence of photothermal effects.

Acknowledgment

The authors would like to thank the Research Deputy of Mashhad University of Medical Sciences for the financial support of this research. The results described in this paper are part of an MSc Medical physics thesis.

References

1. Allison RR, Mota HC, Sibata CH. Clinical PD/PDT in North America: An historical review. *Photodiagnosis Photodyn Ther.* 2004;1(4):263-77.
2. Castano AP, Demidova TN, Hamblin MR. Mechanisms in photodynamic therapy: part one—photosensitizers, photochemistry and cellular localization. *Photodiagnosis and Photodynamic Therapy.* 2004;1(4):279-93.
3. Robertson CA, Evans DH, Abrahamse H. Photodynamic therapy (PDT): a short review on cellular mechanisms and cancer research applications for PDT. *Journal of photochemistry and photobiology B, Biology.* 2009;96(1):1-8.
4. Khair A, Chen D, Patil Y, Ma L, Dou QP, Shekhar MPV, et al. Nanoparticle-mediated combination chemotherapy and photodynamic therapy overcomes tumor drug resistance. *Journal of controlled release : official journal of the Controlled Release Society.* 2010;141(2):137-44.
5. Wrzesien-Kus A, Robak T, Jamrozik K, Wierzbowska A, Dmoszynska A, Adamczyk-Cioch M, et al. The treatment of acute myeloid leukemia with mitoxantrone, etoposide and low-dose cytarabine in elderly patients - a report of Polish Acute Leukemia Group (PALG) phase II study. *Neoplasma.* 2002;49(6):405-11.
6. Shpall EJ, Jones RB, Holland JF, Bhardwaj S, Paciucci PA, Wilfinger CL, et al. Intensive single-agent mitoxantrone for metastatic breast cancer. *Journal of the National Cancer Institute.* 1988;80(3):204-8.

7. Armitage JO. The role of mitoxantrone in non-Hodgkin's lymphoma. *Oncology* (Williston Park, NY). 2002;16(4):490-502.
8. Montazerabadi A-R, Sazgarnia A, Bahreyni-Toosi MH, Ahmadi A, Shakeri-Zadeh A, Aledavood A. Mitoxantrone as a prospective photosensitizer for photodynamic therapy of breast cancer. *Photodiagnosis and Photodynamic Therapy*. 2012;9(1):46-51.
9. Feofanov A, Sharonov S, Kudelina I, Fleury F, Nabiev I. Localization and molecular interactions of mitoxantrone within living K562 cells as probed by confocal spectral imaging analysis. *Biophysical journal*. 1997;73(6):3317-27.
10. Foye WO, Vajragupta O, Sengupta SK. DNA-binding specificity and RNA polymerase inhibitory activity of bis (aminoalkyl) anthraquinones and bis (methylthio) vinylquinolinium iodides. *Journal of pharmaceutical sciences*. 1982;71(2):253-7.
11. Bradbury EM, Van Holde K. Chromatin structure and dynamics: a historical perspective. *New Comprehensive Biochemistry*. 2004;39:1-11.
12. He S, Dunn KL, Espino PS, Drobic B, Li L, Yu J, et al. Chromatin organization and nuclear microenvironments in cancer cells. *Journal of cellular biochemistry*. 2008;104(6):2004-15.
13. Hajihassan Z, Rabbani-Chadegani A. Studies on the binding affinity of anticancer drug mitoxantrone to chromatin, DNA and histone proteins. *Journal of biomedical science*. 2009;16(1):31.
14. Homolya L, Orbán TI, Csanády L, Sarkadi B. Mitoxantrone is expelled by the ABCG2 multidrug transporter directly from the plasma membrane. *Biochimica et Biophysica Acta (BBA) - Biomembranes*. 2011;1808(1):154-63.
15. Ho CK, Law SL, Chiang H, Hsu ML, Wang CC, Wang SY. Inhibition of microtubule assembly is a possible mechanism of action of mitoxantrone. *Biochem Biophys Res Commun*. 1991;180(1):118-23.
16. Ho C-K, Law S-L, Chiang H, Hsu M-L, Wang C-C, Wang S-Y. Inhibition of microtubule assembly is a possible mechanism of action of mitoxantrone. *Biochemical and biophysical research communications*. 1991;180(1):118-23.
17. Chavan S, Parekh H, Chitnis M. Antineoplastic activity of mitoxantrone and its biological interactions in parental and multidrug resistant subline of P388 murine leukemia cells. *Neoplasma*. 1992;39(1):49-57.
18. Safa AR, Chegini N, Tseng MT. Influence of mitoxantrone on nucleic acid synthesis on the T-47D breast tumor cell line. *J Cell Biochem*. 1983;22(2):111-20.
19. Kapuscinski J, Darzynkiewicz Z, Traganos F, Melamed MR. Interactions of a new antitumor agent, 1, 4-dihydroxy-5, 8-bis [[2-[(2-hydroxyethyl) amino]-ethyl] amino]-9, 10-anthracenedione, with nucleic acids. *Biochemical pharmacology*. 1981;30(3):231-40.
20. Fanciullino R, Ciccolini J, Milano G. Challenges, expectations and limits for nanoparticles-based therapeutics in cancer: a focus on nano-albumin-bound drugs. *Critical reviews in oncology/hematology*. 2013;88(3):504-13.
21. Brown KR, Walter DG, Natan MJ. Seeding of colloidal Au nanoparticle solutions. 2. Improved control of particle size and shape. *Chemistry of Materials*. 2000;12(2):306-13.
22. Imanparast A, Attaran N, Sazgarnia A. In Vitro Investigation into Plasmonic Photothermal Effect of Hollow Gold Nanoshell Irradiated with Incoherent Light. *Iranian Journal of Medical Physics*. 2018;15(3):161-8.
23. Ren Q-Q, Bai L-Y, Zhang X-S, Ma Z-Y, Liu B, Zhao Y-D, et al. Preparation, Modification, and Application of Hollow Gold Nanospheres. *Journal of Nanomaterials*. 2015;2015:7.
24. Melancon MP, Lu W, Yang Z, Zhang R, Cheng Z, Elliot AM, et al. In vitro and in vivo targeting of hollow gold nanoshells directed at epidermal growth factor receptors for photothermal ablation therapy. *Molecular cancer therapeutics*. 2008;7(6):1730-9.
25. Butcher NJ, Mortimer GM, Minchin RF. Unravelling the stealth effect. *Nature Nanotechnology*. 2016;11:310.
26. Cheng Y, Samia AC, Li J, Kenney ME, Resnick A, Burda C. Delivery and efficacy of a cancer drug as a function of the bond to the gold nanoparticle surface. *Langmuir*. 2009;26(4):2248-55.
27. Coates J. Interpretation of infrared spectra, a practical approach. *Encyclopedia of analytical chemistry*. 2000;12:10815-37.
28. Toh T-B, Lee D-K, Hou W, Abdullah LN, Nguyen J, Ho D, et al. Nanodiamond-Mitoxantrone Complexes Enhance Drug Retention in Chemoresistant Breast Cancer Cells. *Molecular Pharmaceutics*. 2014;11(8):2683-91.
29. Barar J, Kafil V, Majd MH, Barzegari A, Khani S, Johari-Ahar M, et al. Erratum to: Multifunctional mitoxantrone-conjugated magnetic nanosystem for targeted therapy of folate receptor-overexpressing malignant cells. *Journal of Nanobiotechnology*. 2015;13(1):59.
30. Huang X, El-Sayed MA. Plasmonic photo-thermal therapy (PPTT). *Alexandria Journal of Medicine*. 2011;47(1):1-9.